ELSEVIER SAUNDERS

POSITRON EMISSION TOMOGRAPHY

PET Clin 2 (2007) 267–277

Tracer Kinetic Modeling in PET

M'hamed Bentourkia, PhD[a,*], Habib Zaidi, PhD, PD[b]

This article offers an overview of kinetic modeling strategies for a wide range of problems in PET. The emphasis is on practical applications so that one can understand the potential of (and take full advantage of) this imaging modality. The basic concepts are presented in numerous publications and are only briefly discussed here. It has been suggested that if specific imaging protocols are applied to allow the extraction of physiologic parameters, PET imaging could provide an interesting database in clinical and research settings.

Exploring the human anatomy and physiology in vivo and noninvasively for disease prognosis, diagnosis, and assessment of response to treatment and follow-up is the goal of any medical imaging procedure. Virtually all medical imaging modalities operated clinically nowadays are used mainly for the detection of disease by qualitative visual inspection of the images. In research studies, however, the imaging data are quantified and further statistically analyzed before any sensitive conclusions can be drawn. This is about the methodology. What about the modality itself? First, the research is oriented based on the modality that is available to the investigator. Second, the use of any modality requires a strong collaboration between multidisciplinary groups of investigators who have backgrounds in various scientific specialties related to the research subject. For each modality, novel techniques are continuously being developed for the accurate calculation of physiologic parameters and to better exploit the quantitative potential of the imaging modality [1]. Fig. 1 roughly depicts the extent of each imaging modality based on its widespread use [2]. In this review, the authors focus on the various approaches used in PET kinetic modeling procedures.

The kinetic modeling of PET data depends on the radiotracer used for imaging, the data acquisition protocol, and the biologic tissues under study. Each radiotracer behaves differently in the body, and the same tracer could be affected differently in different types of tissue. There are a quasi-unlimited number of PET radiotracers that can be developed. The list of available radiotracers already in use and their applications in a wide variety of imaging-based investigations could fill several pages [3]. This article focuses on the most widely used radiotracers in typical PET studies and deliberately keeps away from discussing PET data correction procedures and image reconstruction techniques that are addressed in other articles found elsewhere in

This work was supported by grant SNSF 3100A0-116547 from the Swiss National Foundation.

[a] Department of Nuclear Medicine and Radiobiology, University of Sherbrooke, 3001, 12th Avenue North, Sherbrooke (Qc) J1H 5N4, Canada

[b] Division of Nuclear Medicine, Geneva University Hospital, CH-1211 Geneva, Switzerland

* Corresponding author.

E-mail address: mhamed.bentourkia@usherbrooke.ca (M. Bentourkia).

1556-8598/07/$ – see front matter

doi:10.1016/j.cpet.2007.08.003

pet.theclinics.com

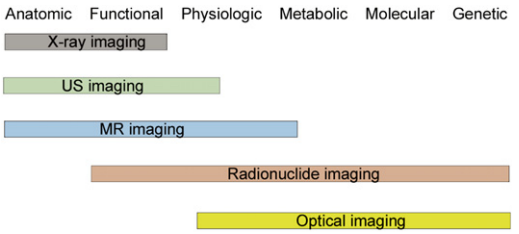

Fig. 1. Extent of the most popular imaging modalities based on their widespread use in imaging applications.

this issue. All the corrections (including decay correction) are assumed to be performed optimally using well-established procedures.

The basis of kinetic modeling

The Fick principle

The Fick (Adolf Eugen Fick, 1829–1901) principle describes the concentration of a substance in a flowing fluid. Suppose that a fluid has a flow F (L/min) and contains a concentration C_1 (mL/L) of a substance. The fluid flows through a compartment that adds the substance in the fluid at a rate M (mL/min). At the exit of the compartment, the fluid has a concentration C_2 (mL/L) of that substance. The Fick principle is then expressed as:

$$C_2 - C_1 = \frac{M}{F} \tag{1}$$

This principle is general and can be applied in several domains. For example, oxygen consumption (MVO_2, milliliters of oxygen per minute per 100 g of tissue) can be obtained from the concentration of oxygen in arterial blood (C_aO_2, milliliters of oxygen per milliliters of blood), from the concentration of oxygen in venous blood (C_vO_2, milliliters of oxygen per milliliters of blood), and from the blood flow (F, milliliters of blood per minute per 100 g of tissue):

$$F(C_aO_2 - C_vO_2) = MVO_2 \tag{2}$$

The Renkin-Crone model

The model of Renkin-Crone [4,5] considers the extraction of a substance from the blood plasma by a tissue. Fig. 2 shows two types of the model. The extraction of the substance from blood is given by

$$E = \frac{C_a - C_v}{C_a} = 1 - \exp\left(-PS/F\right) \tag{3}$$

Suppose that this substance is a radiotracer. The perfusion of the tissue can be accurately measured if the radiotracer is completely extracted from blood after each pass in the capillaries. Several parameters have been used to quantify the passage of the radiotracer from blood to tissue: the extraction (E, unitless); the permeability (P, cm/min); the global blood flow (F, mL/min); the local blood flow (mL/min/100 g); the perfusion (blood flow per volume of tissue, mL/min/g); the transit time; the volume of distribution (V_d); the partition coefficient (r); the clearance (C_r); and the rate constant (K_1, equivalent to the perfusion, mL/g/min). One should not confound the flow in the capillaries with the blood flow in large vessels in which the blood circulation is higher.

The Kety-Schmidt model

Kety and Schmidt [6,7] described their model using nonradioactive substances in the 1940s. The model is based on the Fick model, which stipulates that the extracted substance by a tissue (dC_t/dt) comes from the difference between the arterial (C_a) and venous (C_v) concentrations of this substance:

$$\frac{dC_t}{dt} = F(C_a - C_v) \tag{4}$$

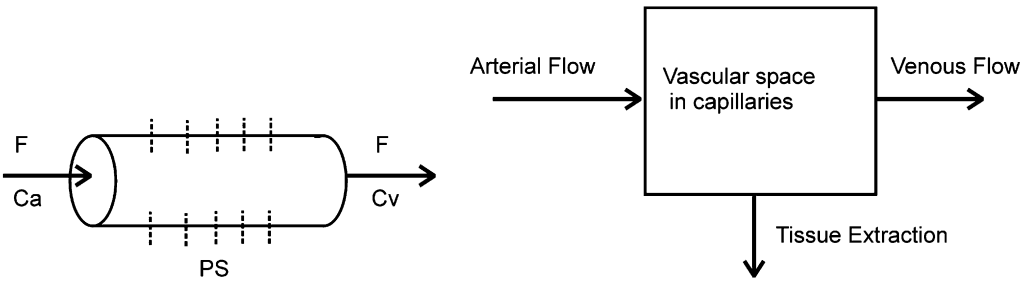

Fig. 2. Diagram showing the concentration of a substance in arterial blood (Ca, μmol/L of blood) and in venous blood (Cv, μmol/L of blood), the local blood flow (F, mL/min/100 g), and the product of the permeability P (cm/min) with the surface S (cm^2/g of tissue) of the capillaries (density of tissue = 1.04 g/cm^3, or 1 mL of tissue = 1.04 g).

The concentration of the substance in tissue was difficult to assess. These investigators supposed that there is a moment when the concentration of the substance in tissue and in venous blood is in equilibrium. Meanwhile, the concentrations should be linked to the tissue volume and to the venous blood volume. This relation is expressed by the volume of distribution (V_d) and by the partition coefficient (p) (Fig. 3).

After the partition coefficient is known, the concentration of the substance in tissue is deduced from the concentration of the substance in the venous blood (or vice versa):

$$C_t = p\, C_v \tag{5}$$

In nuclear medical imaging, it is possible to measure the radiotracer concentration in tissue and in arterial blood [8,9]. Equation 4 then becomes

$$\frac{dC_t}{dt} = FC_a - \frac{F}{p}C_t \tag{6}$$

The solution of this equation [8,10,11] is given by

$$C(t) = F\int_0^t C_a(t')\exp\left(-\frac{F}{p}(t-t')\right)dt' \tag{7}$$

Equation 7 can be rewritten in a simple fashion using the convolution operator denoted $\otimes$:

$$C_t(t) = F\, C_a(t) \otimes \exp\left(-\frac{F}{p}t\right) \tag{8}$$

Equation 8 is the common equation used to calculate the blood flow with the freely diffusible radiotracer $H_2{}^{15}O$. From Equation 8, one can get

$$C_t(t) = F\int_0^t C_a(t')\,dt' - k\int_0^t C_t(t')dt' \tag{9}$$

where k is equal to F/p. By dividing left and right members of Equation 9 with the integral of $C_a(t)$, one can obtain

$$\frac{C_t(t)}{\int_0^t C_a(t')\,dt'} = F - k\frac{\int_0^t C_t(t')\,dt'}{\int_0^t C_a(t')\,dt'} \tag{10}$$

This equation is in the form $y = ax + b$ and is easy and fast to compute for each voxel in the image, leading to a parametric map of blood flow.

Recall that this model is valid under certain conditions [10]:

- The radiotracer should be inert
- The radiotracer should be freely and rapidly diffusible and should be extracted at first pass in the capillaries. The extraction should be rapid in comparison to the transit time of the radiotracer in the capillaries.
- The concentrations of the radiotracer in tissue and in venous blood should be in equilibrium.
- The blood flux should remain constant during the measurements.
- The tissue needs to be homogeneous versus blood flux.

The reader is referred to the article published by Matthews and colleagues [11] in which the approach of Kety and Schmidt [6,7] was used in the assessment of cerebral blood flow.

The input function

Knowledge of the input function is mandatory in PET kinetic modeling. The input function represents the delivery of the radiotracer to a site of interest, which is then measured with PET. If the input

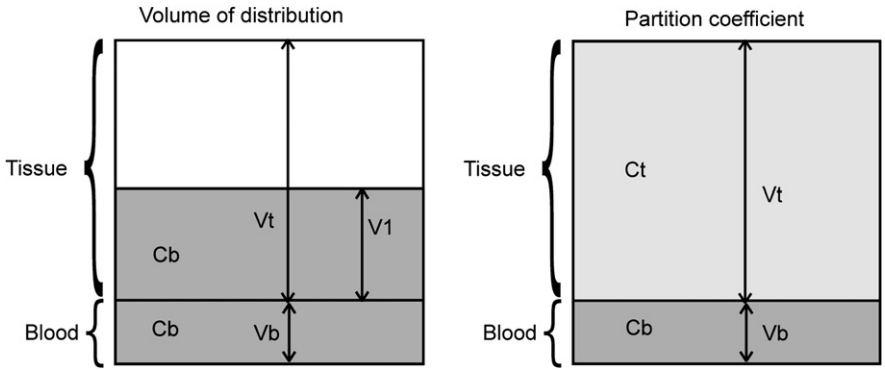

Fig. 3. The volume of distribution (Vd) is the volume of tissue (V1) that should contain the same concentration as in blood (Cb) relative to total tissue volume (Vt): Vd = V1/Vt. The partition coefficient (p) represents the ratio of the concentrations in tissue and in blood: p = Ct/Cb, by assuming uniform concentrations in whole tissue and in blood.

function is viewed as the impulse and the PET measurement in a tissue viewed as the response, then the way the tissue responds to the impulse will depend on how the radiotracer is biochemically transformed in the tissue. The molecule of the radiotracer may be degraded or may be recombined back. Each transformation, depending on the time each transformation takes, can be represented by a specific function. The transformations can also be represented by compartments. If the radiotracer is injected as a bolus, then the response of the tissue is generally described by exponentials.

The input function determines the radiotracer in the blood (or plasma) delivered to tissue, which can be assessed from arterial blood samples. Blood sampling from arteries that are not reachable or from heated or unheated veins, however, is a burdensome procedure, with risk of radiation exposure for operators and risk of infection, bleeding, and thrombosis for patients [12,13]. Furthermore, placing catheters in the arms of the patients makes them uncomfortable; in small animals, this operation is difficult and there may not be enough blood to extract, especially in repetitive studies. But how accurate is the input function determined from blood sampling? The samples have to be withdrawn manually or automatically by means of blood samplers in a discrete or continuous fashion [14–20]. Moreover, the withdrawn blood samples need to be subsequently interpolated to match the PET scan times. Additional corrections are compulsory to accurately define the input curve, such as the time delay and dispersion in the tubing, the contamination of the samples in the tubing, and the cross-calibration between sample detection setup and the PET scanner [21]. To avoid the difficulties encountered in withdrawing and measuring the blood samples in each patient, and when performing studies in similar protocols, population-based input functions have been used, which are sufficient for many applications. For these functions to be properly applied in kinetic modeling, only one or a few blood samples are extracted from the patient to normalize the averaged input functions [22–24]. Because population-based input functions still need blood sampling, other methods have relied on extraction of the input functions from images [25–28]. This approach could be straightforward in cardiac imaging in which the radioactivity in the arterial blood can be assessed from the left ventricle chamber or from the left atrium. The data can be corrected for the spillover from blood to tissue or from tissue to blood and for the metabolites, but more analyses have to be made (eg, in the case of fluorodeoxyglucose F18-[FDG] in which the plasma curve is needed instead of the whole-blood curve). For imaging other organs, the same procedures have been proposed in defining the input curve from PET images; however, in these cases, the blood function has been obtained from regions of interest (ROIs) on artery images. It is unfortunate that all blood vessels in the images are affected by the partial volume effect (PVE), and their intensity is underestimated [29]. Here also, the data need to be further analyzed before accurately defining the input curve. Many investigators have used correction factors derived from phantom studies, MR imaging, CT, or other means to correct for PVE [29–34].

The most significant progress in the determination of the input functions has been seen with methods that do not require blood sampling (although these methods still need to be fully validated). Such methods include reference tissue approaches [35–40] and decomposition of images by means of factor analysis [41–45] or independent component analysis [46,47]. Are the PET images self-sufficient to calculate physiologic parameters? What is the error introduced from analyzing the blood samples: withdrawing blood samples at various times not corresponding to the PET scans, extracting specific volumes of blood or plasma, counting in a well counter, calibrating with the PET scanner, and finally interpolating the data to be used in kinetic modeling? Does one really need to know the absolute values of a physiologic parameter for each quantitative analysis? The answer is obviously no. Suppose one wants to study the effect of activation in the brain or to study tumor response to a treatment in an animal model using FDG. The input function can be derived from an artery in the image. This input curve will be underestimated due to PVE. This underestimation is a multiplicative factor that affects equally the calculated parameter before and after activation or treatment, and usually, the effect of the intervention is reported as a relative difference or gain that will cancel the effect of PVE. Equation 17 reproduces the FDG three-compartment model [48] in which one can expect the influence of the plasma curve $C_p(t)$ on the rate constants (K_1 to k_4, α_1 and α_2) if $C_p(t)$ is underestimated by PVE. To illustrate the effect of errors in the input curve on the quantitative estimates, the authors have applied the FDG kinetic model using nonlinear least squares fitting (Equation 17) to 11 brain regions from PET images and calculated cerebral metabolic rates of glucose (CMRG; Equation 18) using a manually sampled input curve (*bc1*) and the same input curve divided by 5 (*bc5*) and by 10 (*bc10*). The ratio of CMRG calculated using *bc5* to that using *bc1* and the ratio of CMRG calculated using *bc10* to that using *bc1* are displayed in Fig. 4 for the 11 brain regions. Obviously, the PVE directly affects the physiologic parameter estimate. Nevertheless, what could be

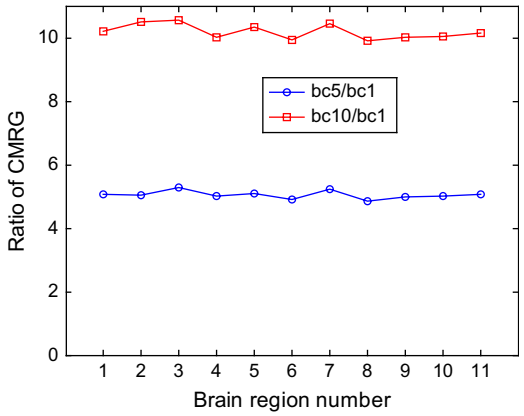

Fig. 4. The underestimation of the input curve by a factor of 5 and a factor of 10 are translated in an overestimation of the CMRG by these factors.

interesting is the response of the tissue after the administration of the radiotracer, and this response is represented by the exponential functions (Equations 8 and 17). In Equation 8, the power of the exponential gives the perfusion regardless of the amplitude, meaning this will depend on the shape of the input function but not on its amplitude. Meanwhile, the calculation of the perfusion (K_1 for FDG and for other radiotracers such as ^{13}N-ammonia and ^{11}C-acetate) directly depends on the amplitude of the input function.

Kinetic modeling approaches

Kinetic modeling is the last process in the analysis and treatment of PET data before the application of statistical analysis. For improved accuracy, kinetic modeling can be done on ROIs because the grouped time-activity curves of the voxels contribute to the reduction of statistical noise. Kinetic modeling can also be performed on an image voxel basis, thus providing a parametric image. When applying a kinetic model on a voxel basis, the background should be removed from the image because not all voxels obey the kinetic model, and keeping them can generate erroneous results. The intensity of the voxels fluctuates depending on the dose of the radiotracer administered, the physical half-life of the radiotracer, the biologic half-life (ie, uptake and clearance of the tracer from the body), the time frame, the detection efficiency, and PET scanner sensitivity, among other factors. All these factors contribute to the noise in the final parametric image. Fitting the image voxels is also time-consuming, and several techniques have been reported aiming to simplify these procedures; for example, for FDG, the standard (or standardized) uptake value (SUV) [49–51], the fractional uptake rate (FUR) [52–54], graphic analysis [55], and the autoradiographic technique [48,56,57]. Similar or equivalent approaches can be used with other radiotracers. SUV and FUR are called semiquantitative methods. It should be noted that the term *quantification* has been used in several ways in the functional imaging literature [58]. In reality, these methods can be considered quantitative because the calculations return values from the processed images; however, what do these values represent and how accurate and specific are they? More refined quantitative methods are more widely accepted; however, they are thought to be difficult because they require complicated calculations. These methods find their origin in the compartmental representation of the behavior of the radiotracer in the body. Other methods can be used equally for any radiotracer without being related to compartments. These methods are powerful; however, they still need to be validated, given that the extracted parameters have to clearly reflect physiologic parameters (eg, the spectral analysis [59–61] and the maximum likelihood techniques [62,63]). Several publications have addressed the issue of kinetic modeling in the projection-space, where only parametric images are reconstructed [60–67]. Some of these techniques are described in the following subsections. Interested readers are encouraged to consult the previously cited references for in-depth details. The authors use FDG as an example because it remains the most widely used radiotracer in PET.

The classic models

Standardized uptake value

The SUV (also known as the differential uptake ratio, dose uptake ratio, differential absorption ratio, or dose absorption ratio) allows one to evaluate the radiotracer uptake in an ROI, usually a tumor [49,51]. SUV calculations (SUV is unitless) are very fast and require only the knowledge of the radiotracer concentration in an ROI (C_{PET} in MBq/g of tissue), the injected dose (*Dose* in MBq), and the subject weight (w in g):

$$SUV = \frac{C_{PET}}{(Dose/w)} = \frac{C_{PET}w}{Dose} \qquad (11)$$

The quantities C_{PET} and *Dose* need to be corrected for radioactive decay at the beginning of the radiotracer injection. C_{PET} has to be evaluated in a time window, whereas the radiotracer is in a steady state (minimal variation) in tissue.

The SUV is influenced by several parameters [68–72]: (1) the nature of the body weight (ie, the radiotracer is not distributed in the body equally in tissue and in fat); (2) the ROI drawing is very subjective; (3) the PVE and spillover affect the C_{PET} value; (4) the uptake and metabolism of the radiotracer in tissue is influenced by metabolic or hormonal processes in blood; and (5) the non–steady state of

the radiotracer in tissue during the time of C_{PET} measurement provokes uncertainties [68,69]. Nevertheless, Strauss and colleagues [73] demonstrated that the SUV is highly correlated to blood volume, perfusion (K_1), and influx $[(K_1 \times k_3)/(k_2 + k_3)]$ in PET-FDG studies.

To circumvent the limitations of the SUV, other semiquantitative indices have also been proposed. One such index is the specific uptake size index (SUSI), which measures the total uptake of an organ or tissue and can be related in absolute terms to the total activity injected or the specific activity in a reference region [74]. The SUSI is defined as $SUSI = T_s/C_r$, where T_s is the specific uptake in the object and C_r is the concentration per unit volume in the reference region or average body concentration. This index was claimed to be independent of the spatial resolution of the imaging system and the ROI delineated by the user; thus, it might be of potential value in reducing variation in quantitative assessment of tracer uptake in selected regions [75,76].

Fractional uptake rate

The FUR, also called retention index, is computationally similar to the SUV. It is simple and fast and can be applied on selected ROIs or at the voxel level [52–54]. The input function, however, is needed:

$$FUR = \frac{C_{PET}(T)}{\int_0^T C_p(t)\,dt} \tag{12}$$

T is the mean scan time of the static PET measurement C_{PET}. The FUR has a unit of min^{-1}; meanwhile, an index of glucose metabolism (FURGlc; µmol/100 g/min) can be deduced from the FUR [54]:

$$FURGlc = \frac{gl}{LC} FUR \tag{13}$$

Fludeoxyglucose F18 original model

FDG and glucose share the same transport across the blood-brain barrier. They can return back to the plasma or they can move to the phosphorylation compartment. FDG, however, cannot be further transformed as glucose. It can be retained as FDG-6-p or be dephosphorylated and travel back to blood (Fig. 5). The mathematical representation of Fig. 5 can be written as [48]:

$$\begin{aligned} \frac{dC_f(t)}{dt} &= K_1 C_p(t) - (k_2+k_3)C_f(t) + k_4 C_m(t) \\ \frac{dC_m(t)}{dt} &= k_3 C_f(t) - k_4 C_m(t) \end{aligned} \tag{14}$$

The solution of this equation is given by:

$$\begin{aligned} C_f(t) &= \tfrac{K_1}{\alpha_2-\alpha_1}[(k_4-\alpha_1)e^{-\alpha_1 t} + (\alpha_2 - k_4)e^{-\alpha_2 t}] \otimes C_p(t) \\ C_m(t) &= \tfrac{K_1 k_3}{\alpha_2-\alpha_1}(e^{-\alpha_1 t} - e^{-\alpha_2 t}] \otimes C_p(t) \end{aligned} \tag{15}$$

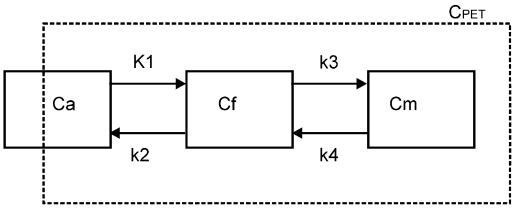

Fig. 5. Ca, Cf, and Cm are the compartments of FDG in blood in the interstitial and metabolized states. K1 is the perfusion (mL/min/g). The other rate constants are in units of min^{-1}. The frame in the dashed line (CPET) represents the voxel or ROI time activity curve.

where $C_p(t)$ is the plasma curve, or the FDG concentration in the plasma. The symbol ⊗ represents the convolution operator. The constants α_1 and α_2 represent combinations of the rate constants:

$$\begin{aligned} \alpha_1 &= [k_2+k_3+k_4 - \sqrt{(k_2+k_3+k_4)^2 - 4k_2k_4}]/2 \\ \alpha_2 &= [k_2+k_3+k_4 + \sqrt{(k_2+k_3+k_4)^2 - 4k_2k_4}]/2 \end{aligned} \tag{16}$$

The sum of $C_f(t)$ and $C_m(t)$ plus a fraction k_5 $(0 \le k_5 < 1)$ of $C_p(t)$ produce the measured data C_{PET} (k_5 is called the blood volume or tissue vascular fraction):

$$\begin{aligned} C_{PET}(t) = \frac{K_1}{\alpha_2-\alpha_1}[&(k_3+k_4-\alpha_1)e^{-\alpha_1 t} \\ &+(\alpha_2 - k_3 - k_4)e^{-\alpha_2 t}] \otimes C_p(t) + k_5 C_p(t) \end{aligned} \tag{17}$$

Knowing $C_{PET}(t)$ and $C_p(t)$ on several time points, it is possible to determine the parameters K_1 to k_5 by least squares fitting or by other means. The metabolic rate for glucose (MRGlc) can be obtained by:

$$\begin{aligned} \text{MRGlc (µmol/100 g/min)} &= \frac{gl(\text{mg of glucose/100 mL of plasma})}{LC\ 0.182\ (\text{mg/ µmol})} \\ &\frac{K_1(\text{mL/g/min})\,k_3(1/\text{min})}{k_2(1/\text{min})+k_3(1/\text{min})} \end{aligned} \tag{18}$$

where gl is the concentration of glucose in plasma and LC is the lumped constant. MRGlc is in micromoles of glucose per 100 g of tissue per minute. Sometimes, MRGlc can be expressed in milliliters of tissue instead of grams of tissue. The factor 0.182 in the denominator accounts for the molecular mass of FDG, which is 182 g/mol.

Fludeoxyglucose F18 autoradiographic model

This method allows one to simplify the PET measurement with FDG and the data analysis procedure. The PET measurement is performed in a single frame after the radiotracer injection to allow an optimal radiotracer uptake in tissue. The modeling can be applied to ROIs or performed at the voxel level. The method consists of generating $C_f(t)$ and $C_m(t)$ FDG compartments using Equation

15, with the measured $C_p(t)$ and values for the rate constants obtained from averaged values in a population (primed rate constants) [48,56]. The calculated compartments and the measured C_{PET} are summed over the time interval T to yield the MRGlc:

$$\text{MRGlc} = \frac{\text{gl}}{\text{LC}}\frac{\text{K}_1\text{k}_3}{\text{k}_2+\text{k}_3} \approx \frac{gl}{LC}\frac{K_1'k_3'}{k_2'+k_3'}\left[\frac{C_{PET}(T)-C_f'(T)}{C_m'(T)}\right] \tag{19}$$

Equation 19 might return negative values for MRGlc. This equation was modified by Hutchins and colleagues [57], who proposed another form of the model:

$$\text{MRGlc} = \frac{\text{gl}}{\text{LC}}\frac{\text{K}_1\text{k}_3}{\text{k}_2+\text{k}_3} \approx \frac{gl}{LC}\frac{K_1'k_3'}{k_2'+k_3'}\left[\frac{C_{PET}(T)}{C'_f(T)+C'_m(T)}\right] \tag{20}$$

Fludeoxyglucose F18 graphic analysis

The graphic analysis was developed by Patlak and colleagues [55]. It is often referred to as the Patlak plot or the Patlak method. This kind of analysis was selectively applied to FDG [77] but can be applied equally well to other radiotracers (eg, ^{13}N-ammonia [78]). The method assumes that $k4$ is null; thus, Equation 16 becomes:

$$\begin{aligned}\alpha_1 &= 0\\ \alpha_2 &= k_2+k_3\end{aligned} \tag{21}$$

and if the last term is omitted, then Equation 17 becomes:

$$C_{PET}(t) = \frac{K_1}{k_2+k_3}\left[k_3+k_2\, e^{-(k_2+k_3)t}\right]\otimes C_p(t) \tag{22}$$

Considering $C_p(t)$ constant relative to the exponential,

$$C_{PET}(t) = \frac{K_1}{k_2+k_3}\left[k_3\int_0^t C_p(u)\,du + \frac{k_2}{k_2+k_3}C_p(t)\right] \tag{23}$$

and dividing both sides by $C_p(t)$, gives

$$C_{PET}(t)/C_p(t) = \frac{K_1k_3}{k_2+k_3}\int_0^t C_p(u)du/C_p(t) + \frac{K_1k_2}{(k_2+k_3)^2} \tag{24}$$

This equation is in the form $y = ax + b$, where the slope $\frac{K_1k_3}{k_2+k_3}$ can be calculated from the last data points made of the most contrasted tissue in the image. This expression is given in Equation 18.

Spectral analysis

Spectral analysis is based on the decomposition of the response of tissue after a bolus injection of a radiotracer in all the possible components. As discussed earlier and as demonstrated by the equations governing a radiotracer kinetic model, the response of a tissue has an exponential form. For example, ^{15}O-water is governed by one exponential (Equation 8), whereas FDG is governed by two exponentials (Equation 17). The number of exponentials is defined for a homogeneous tissue; in fact, they represent the number of compartments. If an ROI or a voxel is made of a mixture of N tissue components, then the time-activity curve of this ROI would be formed by 2N compartments or exponentials, in the case of FDG. This is more realistic if we know that the ROI could be contaminated because of the limited spatial resolution of the PET scanner and the motion of the measured subject. In spectral analysis, we do not have a priori knowledge of the number of tissue components in the ROI or the number of compartments of the radiotracer, whereas the input function must be known. Suppose the macroparameters in Equation 17 are substituted to microparameters, and a single convolution operation is made using the Dirac delta function δ and $A_0 = k_5$:

$$C_{PET}(t) = \left[A_1e^{-B_1t}+A_2e^{-B_2t}+A_0\delta\right]\otimes C_p(t) \tag{25}$$

If there are N time points or data frames, then the convolution with the first two functions gives 2N − 1 data points. One needs to keep only the first N data points. The spectral analysis consists of generating M values of B that makes M exponentials that are subsequently convolved with $C_p(t)$. Consequently, one obtains M values for A, and Equation 25 can be written as

$$\text{Cpet(t1, t2, t3, …, tN)} = [\text{A1 A2 A3…AM}]\begin{vmatrix} \text{F11, F12, F13, …, F1N}\\ \text{F21, F22, F23, …, F2N}\\ \text{F31, F32, F33, …, F3N}\\ \\ \\ \text{FM1, FM2, FM3, …, FMN}\end{vmatrix} \tag{26}$$

The functions Fij ($i = 1$ to M and $j = 1$ to N, with M being the number of compartments and N the number of frames) are the products of the exponentials with $C_p(t)$, and the vector Ai ($i = 1$ to M) consists of the coefficients to be calculated. The matrix F is known because the exponentials are known, and C_{PET} is the time-activity curve of the ROI or voxel. A solution with non-negative least squares produces the values of the coefficients in A. The algorithm of the non-negative least squares giving the solution of A generates a matrix of all possible values of A and zeros elsewhere. The indices of A where $A = 0$ allows one to identify and reject all values of B. A few values of A and B are isolated to form the functions in Equation 25 that really fit $C_{PET}(t)$.

As an example based on the work given by Bentourkia [61], suppose that there are $nb = 50$ compartments (ie, 50 exponentials). One then needs to decide the minimum and maximum values of b; for instance, $bmin = -5$ and $bmax = 0$. The steps are then defined as $(bmax - bmin)/nb$. So, b goes from $bmin = -5$ to $bmax = 0$ with $steps = (bmax - bmin)/nb$. The value of B used in the exponentials is defined as $B = 10^b$.

When the vectors A and B are calculated, one can produce any compartment or the blood volume images by computing the specific exponentials convolved with the input function. It is possible to produce images of any A or B value to represent the ratio of that compartment. Note that other approaches use the spectral analysis differently [59,60].

The maximum likelihood

It is tempting to consider an algorithm that directly reconstructs the parametric images (see the article by Reader and Zaidi found elsewhere in this issue). In fact, there is no need to reconstruct so many images with same filtering not adapted to intensity distribution in the images as a function of frame lengths, radiotracer half-life affecting the statistics, and finally, splitting the projection intensities in so many voxels in reconstructed images. In PET imaging, even a single voxel in the image cannot be considered to represent a homogeneous tissue. An ROI is far from being considered a set of homogeneous structures. A projection (ie, a set of parallel lines of response) has higher statistics but contains the sum of all detected coincidences. When an algorithm based on spectral analysis is used, it can be efficient in the projection-space or in the image-space and can isolate each component in the signal. In a similar manner, the maximum likelihood approach was proposed [62] to decompose the signal and to reconstruct individual components:

$$X_{il} = \sum_k W_{ik} B_{kl} \qquad (27)$$

where X_{il} is the i^{th} image pixel of the l^{th} time frame, W_{ik} is the weight of the i^{th} image pixel in the k^{th} kinetic component, and B_{kl} represents the value of the k^{th} kinetic component in the l^{th} time frame.

Despite the difficulties in simultaneously handling image reconstruction and kinetic modeling, Kamasak and colleagues [63] reported that they successfully reconstructed kinetic parameters (not kinetic components) directly from the projections. This is probably the best way to exploit PET imaging modality to its highest potential (ie, to directly reconstruct images representing kinetic or, more precisely, physiologic parameters). A single-intensity image could also be concurrently produced for global information.

Summary

This article presents the basic principles in clinical and research applications of kinetic modeling, which can be applied to various dynamic PET data. Two main difficulties can arise when selecting a particular compartmental model: the number of identifiable components is fewer than the chosen model (eg, high noise) or more than the chosen model (eg, heterogeneity). Different strategies have been suggested to tackle these problems.

It is gratifying to see the overall the progress that kinetic modeling has made in the last 2 decades. Recent developments have been enormous, particularly in the last few years, with the main efforts striving to improve the accuracy and precision of the computations and to decrease the amount of input data required by the model. The application of kinetic modeling is well established in research environments but limited in clinical settings to those institutions having advanced physics and technical support. As the aforementioned challenges are met and experience is gained, implementation of validated techniques in commercial software packages will be useful to attract the interest of the clinical community and to increase the popularity of these tools. It is expected that with the availability of advanced mathematical models and computing power in the near future, more complex and ambitious kinetic modeling algorithms will become clinically feasible.

References

[1] Basu S, Zaidi H, Houseni M, et al. Novel quantitative techniques for assessing regional and global function and structure based on modern imaging modalities: implications for normal variation, aging and diseased states. Semin Nucl Med 2007;37:223–39.
[2] Cherry S. In vivo molecular and genomic imaging: new challenges for imaging physics. Phys Med Biol 2004;49:R13–48.
[3] Fowler JS, Ding YS, Volkow ND. Radiotracers for positron emission tomography imaging. Semin Nucl Med 2003;33:14–27.
[4] Renkin EM. Transport of potassium-42 from blood to tissue in isolated mammalian skeletal muscles. Am J Physiol 1959;197:1205–10.
[5] Crone C. Facilitated transfer of glucose from blood into brain tissue. J Physiol 1965;181:103–13.
[6] Kety SS, Schmidt CF. The determination of cerebral blood flow in man by the use of nitrous oxide in low concentrations. Am J Physiol 1945;143:53–66.

[7] Kety SS, Schmidt CF. The nitrous oxide method for the quantitative determination of cerebral blood flow in man: theory, procedure and normal values. J Clin Invest 1948;27:476–83.
[8] Duncan CC, Lambrecht RM, Rescigno A, et al. The ramp injection of radiotracers for blood flow measurement by emission tomography. Phys Med Biol 1983;28:963–72.
[9] MacVeigh I, Cook DJ, Orszulak TA, et al. Nitrous oxide method of measuring cerebral blood flow during hypothermic cardiopulmonary bypass. Ann Thorac Surg 1997;63:736–40.
[10] Koeppe RA, Holden JE, Ip WR. Performance comparison of parameter estimation techniques for the quantitation of local cerebral blood flow by dynamic positron computed tomography. J Cereb Blood Flow Metab 1985;5:224–34.
[11] Matthews J, Matthews D, Eyre J. Statistical method for the estimation of cerebral blood flow using the Kety-Schmidt technique. Clin Sci 1999;97:485–92.
[12] Bedford RF, Wollman H. Complications of percutaneous radial-artery cannulation: an objective prospective study in man. Anesthesiology 1973; 38:228–36.
[13] Jons PH, Ernst M, Hankerson J, et al. Follow-up of radial arterial catheterization for positron emission tomography studies. Hum Brain Mapp 1997;5:119–23.
[14] Hutchins R, Hichiwa R, Koeppe R. A continuous flow input function detector for $H_2{}^{15}O$ blood flow studies in positron emission tomography. IEEE Trans Nucl Sci 1986;33:546–9.
[15] Iida H, Kanno I, Miura S, et al. Error analysis of a quantitative cerebral blood flow measurement using H2(15)O autoradiography and positron emission tomography, with respect to the dispersion of the input function. J Cereb Blood Flow Metab 1986;6:536–45.
[16] Senda M, Nishizawa S, Yonekura Y, et al. Measurement of arterial time-activity curve by monitoring continuously drawn arterial blood with an external detector: errors and corrections. Ann Nucl Med 1988;2:7–12.
[17] Ranicar AS, Williams CW, Schnorr L, et al. The on-line monitoring of continuously withdrawn arterial blood during PET studies using a single BGO/photomultiplier assembly and non-stick tubing. Med Prog Technol 1991;17:259–64.
[18] Tadokoro H, Yoshida K, Takami A, et al. A high detection efficiency BGO, flow-through, coincidence detection system for arterial blood sampling with PET: application and dispersion correction for small animal PET studies. IEEE Nuclear Science Symposium 1997;2:1528–32.
[19] Boellaard R, van Lingen A, van Balen SC, et al. Characteristics of a new fully programmable blood sampling device for monitoring blood radioactivity during PET. Eur J Nucl Med 2001;28: 81–9.
[20] Convert L, Morin-Brassard G, Cadorette J, et al. A new tool for molecular imaging: the microvolumetric {beta} blood counter. J Nucl Med 2007;48:1197–206.
[21] Dhawan V, Jarden J, Strother S, et al. Effect of blood curve smearing on the accuracy of parameter estimates obtained for 82Rb/PET studies of blood-brain barrier permeability. Phys Med Biol 1988;33:61–74.
[22] Takikawa S, Dhawan V, Spetsieris P, et al. Noninvasive quantitative fluorodeoxyglucose PET studies with an estimated input function derived from a population-based arterial blood curve. Radiology 1993;188:131–6.
[23] Eberl S, Anayat AR, Fulton RR, et al. Evaluation of two population-based input functions for quantitative neurological FDG PET studies. Eur J Nucl Med 1997;24:299–304.
[24] Wakita K, Imahori Y, Ido T, et al. Simplification for measuring input function of FDG PET: investigation of 1-point blood sampling method. J Nucl Med 2000;41:1484–90.
[25] Gambhir S, Schwaiger M, Huang S, et al. Simple noninvasive quantification method for measuring myocardial glucose utilization in humans employing positron emission tomography and fluorine-18 deoxyglucose. J Nucl Med 1989;30: 359–66.
[26] Iida H, Rhodes C, de Silva R, et al. Use of the left ventricular time-activity curve as a noninvasive input function in dynamic oxygen-15-water positron emission tomography. J Nucl Med 1992; 33:1669–77.
[27] Yoshida K, Endo M, Fukuda G, et al. Measurement of arterial tracer concentrations from cardiac PET images. J Comput Assist Tomogr 1995;19:182–7.
[28] Lin K, Huang S, Choi Y, et al. Correction of spillover radioactivities for estimation of the blood time-activity curve from the imaged LV chamber in cardiac dynamic FDG PET studies. Phys Med Biol 1995;40:629–42.
[29] Rousset OG, Rahmim A, Alavi A, Zaidi H. Partial volume correction strategies in PET. PET Clin, in press.
[30] Ohtake T, Kosaka N, Watanabe T, et al. Noninvasive method to obtain input function for measuring tissue glucose utilization of thoracic and abdominal organs. J Nucl Med 1991;32: 1433–8.
[31] Germano G, Chen B, Huang S, et al. Use of the abdominal aorta for arterial input function determination in hepatic and renal PET studies. J Nucl Med 1992;33:613–20.
[32] Litton J. Input function in PET brain studies using MR-defined arteries. J Comput Assist Tomogr 1997;21:907–9.
[33] Hoekstra C, Hoekstra O, Lammertsma A. On the use of image-derived input functions in oncological fluorine-18 fluorodeoxyglucose positron emission tomography studies. Eur J Nucl Med 1999;26:1489–92.
[34] Watabe H, Channing M, Riddell C, et al. Noninvasive estimation of the aorta input function for

measurement of tumor blood flow with 15O-water. IEEE Trans Med Imaging 2001;20:164–74.
[35] Lammertsma AA, Hume SP. Simplified reference tissue model for PET receptor studies. Neuroimage 1996;4:153–8.
[36] Gunn RN, Lammertsma AA, Hume SP, et al. Parametric imaging of ligand-receptor binding in PET using a simplified reference region model. Neuroimage 1997;6:279–87.
[37] Parsey R, Slifstein M, Hwang D, et al. Validation and reproducibility of measurement of 5-HT1A receptor parameters with [carbonyl-11C]WAY-100635 in humans: comparison of arterial and reference tissue input functions. J Cereb Blood Flow Metab 2000;20:1111–33.
[38] Gunn RN, Gunn SR, Cunningham VJ. Positron emission tomography compartmental models. J Cereb Blood Flow Metab 2001;21:635–52.
[39] Millet P, Graf C, Buck A, et al. Evaluation of the reference tissue models for PET and SPECT benzodiazepine binding parameters. Neuroimage 2002;17:928–42.
[40] Bentourkia M. Kinetic modeling of PET-FDG in the brain without blood sampling. Comput Med Imaging Graph 2006;30:447–51.
[41] Wu H, Huang S, Allada V, et al. Derivation of input function from FDG-PET studies in small hearts. J Nucl Med 1996;37:1717–22.
[42] Bentourkia M, Lapointe D, Selivanov V, et al. Determination of blood curve and tissue uptake from left ventricle using FADS in rat FDG-PET studies. IEEE Nuclear Science Symposium and Medical Imaging Conference Record, Seattle (WA), October 24–30, 1999;2:1124–7.
[43] Ahn J, Lee D, Lee J, et al. Quantification of regional myocardial blood flow using dynamic H2(15)O PET and factor analysis. J Nucl Med 2001;42:782–7.
[44] Frouin F, Merlet P, Bouchareb Y, et al. Validation of myocardial perfusion reserve measurements using regularized factor images of H(2)(15)O dynamic PET scans. J Nucl Med 2001;42: 1737–46.
[45] Bentourkia M. Kinetic modeling of PET data without blood sampling. IEEE Trans Nucl Sci 2005;52:697–702.
[46] Naganawa M, Kimura Y, Ishii K, et al. Extraction of a plasma time-activity curve from dynamic brain PET images based on independent component analysis. IEEE Trans Biomed Eng 2005;52: 201–10.
[47] Naganawa M, Kimura Y, Nariai T, et al. Omission of serial arterial blood sampling in neuroreceptor imaging with independent component analysis. Neuroimage 2005;26:885–90.
[48] Phelps ME, Huang SC, Hoffman EJ, et al. Tomographic measurement of local cerebral glucose metabolic rate in humans with (F-18)2-fluoro-2-deoxy-D-glucose: validation of method. Ann Neurol 1979;6:371–88.
[49] Huang S-C. Anatomy of SUV. Nucl Med Biol 2000;27:643–6.
[50] Lucignani G, Paganelli G, Bombardieri E. The use of standardized uptake values for assessing FDG uptake with PET in oncology: a clinical perspective. Nucl Med Commun 2004;25:651–6.
[51] Thie JA. Understanding the standardized uptake value, its methods, and implications for usage. J Nucl Med 2004;45:1431–4.
[52] Ishizu K, Nishizawa S, Yonekura Y, et al. Effects of hyperglycemia on FDG uptake in human brain and glioma. J Nucl Med 1994;35:1104–9.
[53] Thie JA. Clarification of a fractional uptake concept. J Nucl Med 1995;36:711–2.
[54] Ishizu K, Yonekura Y. Clarification of a fractional uptake concept—reply. J Nucl Med 1995;36:712.
[55] Patlak CS, Blasberg RG, Fenstermacher JD. Graphical evaluation of blood-to-brain transfer constants from multiple-time uptake data. J Cereb Blood Flow Metab 1983;3:1–7.
[56] Sokoloff L. Relation between physiological function and energy metabolism in the central nervous system. J Neurochem 1977;29:13–26.
[57] Hutchins G, Holden J, Koeppe R, et al. Alternative approach to single-scan estimation of cerebral glucose metabolic rate using glucose analogs, with particular application to ischemia. J Cereb Blood Flow Metab 1984;4:35–40.
[58] Van Laere K, Zaidi H. Quantitative analysis in functional brain imaging. In: Zaidi H, editor. Quantitative analysis of nuclear medicine images. New York: Springer; 2006. p. 435–70.
[59] Cunningham V, Jones T. Spectral analysis of dynamic PET studies. J Cereb Blood Flow Metab 1993;13:15–23.
[60] Meikle SR, Matthews JC, Cunningham VJ, et al. Parametric image reconstruction using spectral analysis of PET projection data. Phys Med Biol 1998;43:651–66.
[61] Bentourkia M. PET kinetic modeling of 11C-acetate from projections. Comput Med Imaging Graph 2003;27:373–9.
[62] Matthews J, Bailey D, Price P, et al. The direct calculation of parametric images from dynamic PET data using maximum-likelihood iterative reconstruction. Phys Med Biol 1997;42: 1155–73.
[63] Kamasak ME, Bouman CA, Morris ED, et al. Direct reconstruction of kinetic parameter images from dynamic PET data. IEEE Trans Med Imaging 2005;24:636–50.
[64] Maguire RP, Calonder C, Leenders KL. An investigation of multiple time/graphical analysis applied to projection data: theory and validation. J Comput Assist Tomogr 1997;21:327–31.
[65] Huesman RH, Reutter BW, Zeng GL, et al. Kinetic parameter estimation from SPECT cone-beam projection measurements. Phys Med Biol 1998; 43:973–82.
[66] Yetik IS, Qi J. Direct estimation of kinetic parameters from the sinogram with an unknown blood function. Presented at the 3rd IEEE International Symposium on Biomedical Imaging. Nano to Macro 2006;295–8.

[67] Arhjoul L, Bentourkia M. Assessment of glucose metabolism from the projections using the wavelet technique in small animal pet imaging. Comput Med Imaging Graph 2007;31:157–65.
[68] Keyes JWJ. SUV: standard uptake or silly useless value? J Nucl Med 1995;36:1836–9.
[69] Zasadny KR, Wahl RL. Standardized uptake values of normal tissues at PET with 2-[fluorine-18]-fluoro-2-deoxy-D-glucose: variations with body weight and a method for correction. Radiology 1993;189:847–50.
[70] Kim CK, Gupta N, Chandramouli B, et al. Standardized uptake values of FDG: body surface area correction is preferable to body weight correction. J Nucl Med 1994;35:164–7.
[71] Westerterp M, Pruim J, Oyen W, et al. Quantification of FDG PET studies using standardised uptake values in multi-centre trials: effects of image reconstruction, resolution and ROI definition parameters. Eur J Nucl Med Mol Imaging 2007;34:392–404.
[72] Thie JA, Hubner KF, Isidoro FP, et al. A weight index for the standardized uptake value in 2-deoxy-2-[F-18]fluoro-D-glucose-positron emission tomography. Mol Imaging Biol 2007;9: 91–8.
[73] Strauss LG, Dimitrakopoulou-Strauss A, Haberkorn U. Shortened PET data acquisition protocol for the quantification of 18F-FDG kinetics. J Nucl Med 2003;44:1933–9.
[74] Fleming JS, Bolt L, Stratford JS, et al. The specific uptake size index for quantifying radiopharmaceutical uptake. Phys Med Biol 2004;49:N227–34.
[75] Tossici-Bolt L, Hoffmann SMA, Kemp PM, et al. Quantification of [123I]FP-CIT SPECT brain images: an accurate technique for measurement of the specific binding ratio. Eur J Nucl Med Mol Imaging 2006;33:1491–9.
[76] Montandon M-L, Nozan Z, Zaidi H. Validity of the specific uptake size index (SUSI) in quantitative analysis of clinical 18F-DOPA brain PET studies. Eur J Nucl Med Mol Imaging, in press.
[77] Gjedde A, Wienhard K, Heiss W, et al. Comparative regional analysis of 2-fluorodeoxyglucose and methylglucose uptake in brain of four stroke patients. With special reference to the regional estimation of the lumped constant. J Cereb Blood Flow Metab 1985;5:163–78.
[78] Kitsukawa S, Yoshida K, Mullani N, et al. Simple and Patlak models for myocardial blood flow measurements with nitrogen-13-ammonia and PET in humans. J Nucl Med 1998;39:1123–8.